Published in final edited form as:
Neurobiol Dis. 2015 January ; 73: 83–95. doi:10.1016/j.nbd.2014.08.032.

Intracerebral injection of preformed synthetic tau fibrils initiates widespread tauopathy and neuronal loss in the brains of tau transgenic mice

Eve Peeraer[a], **Astrid Bottelbergs**[a], **Kristof Van Kolen**[a], **Ilie-Cosmin Stancu**[b], **Bruno Vasconcelos**[b], **Michel Mahieu**[a], **Hilde Duytschaever**[a], **Luc Ver Donck**[a], **An Torremans**[c], **Ellen Sluydts**[c], **Nathalie Van Acker**[c], **John A. Kemp**[a], **Marc Mercken**[a], **Kurt R. Brunden**[a], **John Q. Trojanowski**[a], **Ilse Dewachter**[b], **Virginia M.Y. Lee**[a], and **Diederik Moechars**[a,*]

[a] Department of Neuroscience, Janssen Research and Development, A Division of Janssen Pharmaceutica NV, B-2340 Beerse, Belgium

[b] UCLouvain, Institute of Neuroscience, Group of Cellular and Molecular Neuroscience, B-1200 Woluwe-Saint-Lambert, Belgium

[c]*Histogenex, B-2020 Antwerp, Belgium*

[d] Center for Neurodegenerative Disease Research, Institute on Aging, Department of Pathology and Laboratory, University of Pennsylvania School of Medicine, Philadelphia, PA 19104, USA

Abstract

Neurofibrillary tangles composed of hyperphosphorylated fibrillized tau are found in numerous tauopathies including Alzheimer's disease. Increasing evidence suggests that tau pathology can be transmitted from cell-to-cell; however the mechanisms involved in the initiation of tau fibrillization and spreading of disease linked to progression of tau pathology are poorly understood. We show here that intracerebral injections of preformed synthetic tau fibrils into the hippocampus or frontal cortex of young tau transgenic mice expressing mutant human P301L tau induces tau hyperphosphorylation and aggregation around the site of injection, as well as a time-dependent propagation of tau pathology to interconnected brain areas distant from the injection site. Furthermore, we show that the tau pathology as a consequence of injection of tau preformed fibrils into the hippocampus induces selective loss of CA1 neurons. Together, our data confirm previous studies on the seeded induction and the spreading of tau pathology in a different tau transgenic mouse model and reveals neuronal loss associated with seeded tau pathology in tau transgenic mouse brain. These results further validate the utility of the tau seeding model in studying disease transmission, and provide a more complete *in vivo* tauopathy model with associated neurodegeneration which can be used to investigate the mechanisms involved in tau aggregation and spreading, as well as aid in the search for disease modifying treatments for Alzheimer's disease and related tauopathies.

* Corresponding author at: Janssen Research and Development, Turnhoutseweg 30, B-2340 Beerse, Belgium. Fax: +32 14 60 61 21. dmoechar@its.jnj.com (D. Moechars)..

Supplementary data to this article can be found online at http://dx. doi.org/10.1016/j.nbd.2014.08.032.

Keywords

Seeding; Spreading; Tau pathology; Cell death

Introduction

An important hallmark of Alzheimer's disease (AD) is the accumulation of insoluble hyperphosphorylated and fibrillized tau in neurofibrillary tangles (NFTs) (reviewed by Ballatore et al., 2007). Since there is a clear correlation between NFT density and cognitive decline, misfolded and aggregated tau is likely a key pathological agent in AD (Arriagada et al., 1992; Gómez-Isla et al., 1997). The hypothesis that tau plays a critical role in AD pathogenesis was further strengthened by the discovery that inherited forms of frontotemporal dementia with Parkinsonism linked to chromosome 17 (FTDP-17) resulted from mutations within the tau gene (Goedert, 2005a; Goedert and Jakes, 2005b). This provided evidence that alterations of tau itself can directly lead to neurodegenerative disease and suggested that tau aggregation in the AD brain could, indeed, be involved in disease onset and progression.

The events leading to tau aggregate formation are not completely understood and were long thought to be entirely cell-autonomous, with protein misfolding occurring independently in many cells. Recent studies have shown, however, that prion-like cell-to-cell spreading mechanisms might be important in the propagation of tau pathology. In AD, tau inclusions occur in a particular brain area and progress in a well-defined predictable manner (Braak and Braak, 1991; Braak et al., 2011) suggesting a prion-like spreading of aggregated tau or tau fragments with altered conformation. Recent studies in cultured cells indicate that exogenously supplied tau preformed fibrils (PFFs) are internalized by cells, likely *via* endocytosis, and seed the recruitment of endogenous tau to adopt misfolded conformations (Frost et al., 2009; Guo and Lee, 2011; Wu et al., 2013; Holmes et al., 2013). Intracellular tau aggregates can be externalized by degenerating axons or somatodendritic compartments, released *via* secretion or through other unknown mechanisms (Saman et al., 2012; Simón et al., 2012; Chai et al., 2012) and can then be taken up by surrounding or interconnected neurons and template the conversion of soluble tau into insoluble aggregates, giving a plausible explanation for the propagation of tau pathology in the AD brain.

Also, *in vivo* studies have demonstrated that the intracerebral injection of both brain extracts from diseased tau transgenic (Tg) mice or synthetic tau PFFs induce spreading of tau pathology in the brain of tau Tg mice (Clavaguera et al., 2009; Iba et al., 2013). These data, together with the observation that tau pathology can spread along anatomically connected networks *via* trans-synaptic transport in the mouse brain (Liu et al., 2012a; de Calignon et al., 2012), provide further evidence for a prion-like spreading mechanism of tau pathology.

In this study, we injected tau PFFs in the hippocampus or frontal cortex of tau Tg mice expressing human mutant P301L tau found in FTDP-17 pedigrees and we observed induction of tau fibrillization and spreading of tau pathology to interconnected brain regions. Notably, since tau pathology as a consequence of injection of tau PFFs induced selective

neuronal loss in the hippocampus, our data provide an *in vivo* model of tau pathological spread with associated neurodegeneration.

Material and methods

Tau Tg mice

Tg tauP301L mice, expressing the longest human tau isoform with the P301L mutation (tau-4R/2 N-P301L) under control of the *thy1* gene promoter were generated as described previously (Terwel et al., 2005). The animals were used for surgery at the age of 3 m, which is 6 m before they develop tau pathology driven solely by the tau trans-gene. Transgenic tau-4R/2N mice, expressing the longest wildtype human tau isoform (Spittaels et al., 1999) and non-Tg mice were used as controls. All experiments were performed in compliance with protocols approved by the local ethical committee.

Generation of tau PFFs from recombinant tau

Truncated human tau fragments containing the four microtubule binding repeat domain (K18; residues Q244-E372 of the longest human tau isoform) with a P301L mutation (abbreviated as K18-PL) were produced in *Escherichia coli* (Tebu-bio, Le Perray-en-Yvelines, France). The fragments are flanked by a Myc tag at their C- or N-terminus. To obtain tau PFFs, tau K18-PL fragments (66 μM) were incubated at 37 °C for 5 days in the presence of 266 μM heparin (MP Biomedicals, Illkirch, France). Afterwards, the fibrillization mixture was centrifuged at 100,000 ×*g* for 1 h. The resulting pellet was resuspended in 100 mM ammonium acetate buffer (pH 7.0) and sonicated before stereotaxic injection. Successful tau fibrillization was confirmed using Thioflavin T fluorescent assay (Sigma).

Stereotaxic surgery

Three months old mice of either sex were deeply anesthetized with isoflurane. Unilateral stereotaxic injections (right hemisphere) were performed in the hippocampus (A/P, −2.5 mm from bregma; L, +2.0 mm; D/V, −2.4 mm) or frontal cortex (A/P, +2.0 mm; L, +2.0 mm; D/V, −2.7 mm). According to the experiments performed the injection volume varied between 2 and 5 μl and was applied at a speed of 1 μl min^{-1}. After injection, the needle was kept in place for an additional 5 min before gentle withdrawal.

Biochemistry

Mice were sacrificed by decapitation in accordance with protocols approved by the local ethical committee. Left and right hemispheres were weighed and homogenized in 6 volumes of homogenization buffer (10 mM Tris; 0.8 M NaCl; 10% sucrose; 1 mM EGTA; pH 7.6). Whole hemispheres were utilized to circumvent variability due to dissection errors to the maximal extend. The homogenate was centrifuged at 27,000 ×*g* for 20 min and 1% N-lauroylsarcosine (Sigma) was added to the supernatant. After 90 min, the solutions were again centrifuged at 150,000 ×*g* for 1 h. The supernatants were kept as sarkosyl-soluble fraction, whereas the pellet containing the sarkosyl-insoluble material was resuspended in homogenization buffer.

Levels of total and phosphorylated tau in the sarkosyl-insoluble fractions were quantified using sandwich ELISA. PT4 (total tau, epitope 215–227, made in-house) and AT8 (pSer202/Thr205, Vandermeeren et al., 1993) were used as a capture antibody and Horseradish Peroxidase (HRP)-conjugated human tau 10 (htau10, epitope 29–36) was applied as a secondary antibody. The signal was measured on an EnVision Multilabel reader after applying QuantaBlu fluorogenic peroxidase substrate solution (Thermo Scientific, Rockford, USA).

Histology and immunohistochemistry

Mice were sacrificed by decapitation in accordance with protocols approved by the local ethical committee; brains were dissected, postfixed in a formalin-based fixative for 24–36 h and embedded in paraffin. For fluorescent labeling, perfusion of the animals and subsequent histological processing were performed as previously described (Bottelbergs et al., 2012; Huyghe et al., 2006). Briefly, following deparaffinization, rehydration, heat induced antigen retrieval in citrate buffer (pH 6.0) and blocking of endogenous peroxidase activity by 3% hydrogen peroxide; the samples were incubated with the primary antibodies. The sources and dilution factors of the different antibodies are listed in Supplementary Table 1. Peroxidase labeled secondary anti-mouse (Jackson Immunoresearch, Suffolk, UK or Dako, Glostrup, Denmark) or anti-rabbit (from Sigma or Dako) antibodies were used in all studies. Labeling for bright field microscopy was performed using 3,3-diaminobenzidine DAB (Dako), while fluorescent labeling was achieved using cyanine 2 or 3 TSA kits (Perkin Elmer Life Sciences, Boston, USA). In case of double fluorescent staining, AT8 antibody was directly labeled with an Alexa 488 fluorophore by the use of a protein labeling kit (Invitrogen Life Technologies, Gent, Belgium) and primary antibodies were applied sequentially. After mounting with Vectashield hard set containing DAPI (Vector Laboratories, Burlingame, USA), slices were analyzed with a LSM510 confocal laser scanning microscope (Carl Zeiss) equipped with an axiocam camera. For brightfield microscopy, slides were counterstained with hematoxylin and bluing reagent, dehydrated and permanently mounted. Virtual images of the DAB labeled sections were made using a Zeiss Mirax Virtual Slide scanner.

Thioflavin S (ThioS) staining was performed to visualize the tau aggregates. Following dewaxing, the tissue sections were incubated in ThioS (1%) and subsequently differentiated in 70% ethanol. Counterstaining was performed using nuclear Hoechst stain. Digital images of ThioS were made using Zeiss Axio Image Z2.

Nissl staining was used to demonstrate neuronal integrity. Following dewaxing, the tissue sections were incubated in 0.2% cresyl violet acetate and subsequently dehydrated in graded ethanol and permanently mounted.

Image analysis of the AT8, GFAP, Iba-1 and ThioS stains was performed using either Definiens analysis software package v1.5 (Definiens AG), Panoramic Viewer software package v1.15 (3DHistech) or AxioVision software package v4.6 (Zeiss). Per sample, predefined regions were manually delineated on the digital images. For each region separately, the % of marker area was measured, defined by the area occupied by all marker labeling that is darker than a user-defined threshold, divided by the total area of the region of

interest and multiplied by 100. The number of healthy neurons in the CA1 region was counted manually using Adobe Photoshop CS4.

Statistical analysis

Statistical analysis of the data was performed using one-way ANOVA or Student's t test in SigmaPlot 12.0 software. Data were expressed as mean ± SEM, and differences with $p < 0.05$ were considered significant.

Results

Intracerebral injection of tau PFFs initiates tau pathology in tau Tg mice

Recent *in vitro* and *in vivo* data support the concept of transmission of tau pathology. To better understand the mechanisms involved and to develop a more complete *in vivo* tauopathy model, tau PFFs were injected in the brain of Tg tauP301L mice. The injected PFFs consist of an aggregated synthetic human tau fragment containing the four micro-tubule binding repeat domain with a P301L mutation (abbreviated as K18-PL) as described previously (Iba et al., 2013). Tau Tg P301L mice, which express the P301L mutant variant of 2N4R human tau, develop tau pathology at around 9 m of age and this pathology is largely restricted to the brainstem (Terwel et al., 2005). Three month old P301L mice were unilaterally injected with aggregated K18-PL into either the hippocampus or frontal cortex. As a first readout for tau pathology, we measured by ELISA the amount of total and phosphorylated (AT8) tau in the sarkosyl-soluble and -insoluble brain fractions of the injected (right) hemisphere at 1, 2 and 3 m after injection. In mice injected with K18-PL in the hippocampus (Fig. 1A) or cortex (Fig. 1B) a signifi-cant amount of total and phosphorylated tau was detected in the insoluble fraction while very little to no insoluble tau was detected in the brain of buffer injected mice. Interestingly, while equal amounts of PFFs were injected, the amount of insoluble tau was significantly higher in cortex injected animals compared to hippocampus injected animals (*i.e.* $2.51 \times 10^{+6}$ *versus* $1.45 \times 10^{+6}$, respectively), suggesting a role of the injection site in the extent of seeded tau pathology. No differences were observed between the 3 analyzed time points, indicative of the fast nature of the developing tau pathology, which peaked at 1 m after injection. The amount of total tau in the sarkosyl soluble brain fraction was similar in buffer and K18-PL injected brains, whereas the AT8 signal in the sarkosyl soluble brain fraction showed a small increase after injection of K18-PL in the hippocampus (Fig. 1A) and cortex (Fig. 1B), indicating that a small portion of the sarkosyl-soluble tau is also phosphorylated after K18-PL injection.

To investigate the spatial pattern of the developing tau pathology in the injected hemisphere, AT8 immunohistochemistry (IHC) was performed on sagittal brain sections at the level of injection. Delivery of aggregated K18-PL to the hippocampus induced clear tau pathology around the site of injection (hippocampus and cortex above the hippo-campus), which was clearly observed 1 m after injection and did not further increase in the later time points (Figs. 2A–C). Intriguingly, in the piriform cortex, a brain area located more distantly from the injection site, AT8 labeling was not detectable at the 1 and 2 month time point. However, 3 m after injection, phosphorylated tau pathology was significantly induced in this brain area as well. Similar results were obtained with AT100 IHC that detects pT212/pS214

within tau, whereas buffer injected animals were negative for both AT8 and AT100 (data not shown). Likewise, injection of PFFs in the frontal cortex induces tau pathology in the injected hemisphere, however, distribution of pathology is clearly different (Figs. 2D–F). The most profound AT8 labeling was detected around the injection site, but was also obvious in other areas such as the hippocampus, amygdala, thalamus, midbrain and brainstem. Maximal AT8 labeling in the frontal cortex and amygdala was already reached 1 m after injection, whereas tau pathology in the hippocampus, thalamus and midbrain increased with time. Interestingly, no AT8 signal was detected in the brainstem at early time points (1 and 2 m after injection), but tau pathology was clearly induced 3 m after PFFs injection. Similar results were obtained with AT100 IHC (data not shown). The regional differences noted in seeding do not reflect differences in transgene expression since HT7 IHC showed an equal distribution of human tau throughout the entire brain of the tauP301L mouse (data not shown). Overall, these data indicate that intracerebral injections with PFFs induce tau pathology in a variety of brain areas which differ according to the injection site. Furthermore, some areas connected to the site of injection show a clear time-dependent increase in tau pathology, which further corroborates the spreading hypothesis.

Since AT8 and AT100 labelings are indicative of tau pathology in Tg mice injected with PFFs, we next investigated whether we can also detect mature tau tangles by ThioS histochemistry. Mice injected with K18-PL aggregates in the hippocampus showed ThioS-positive tangle formation around the site of injection (Figs. 3A–B), while no other regions were significantly affected up to 3 m after injection (data not shown). Intriguingly, the most ThioS-positive cells in the hippocampus were observed 1 m after tau PFF injection, whereas the number of ThioS-positive cells was lower at 2 or 3 m than at 1 m after injection. Similar results were obtained by Bielschowsky silver stain (Suppl. Fig. 1). This might be an indication for tau tangle clearance or selective neuronal cell loss in the hippocampus. ThioS analysis in mice injected with K18-PL aggregates in the frontal cortex also revealed robust labeling at the site of injection (Figs. 3C–D), with some ThioS labeling also observed in more distal areas such as the hippocampus. Furthermore, the number of ThioS-positive tau aggregates did not decrease in the frontal cortex over the analyzed 3 m post-PFF injection period. In conjunction with the AT8 signal in sarkosyl insoluble fractions of PFF injected mice, these data thus indicate that PFF injection induces hyperphosphorylation and aggregation of Tg human tau, as well as the formation of more mature tau tangles that exhibit histological properties of β-sheet conformation similar to authentic AD tangles.

Tau pathology is also induced in the contralateral hemisphere

Since injection of PFFs induces widespread tau pathology in the injected hemisphere, we next analyzed whether tau phosphorylation and aggregation can also be detected in the contralateral (left) hemisphere. First, we assessed the amount of total and phosphorylated tau in the sarkosyl-soluble and -insoluble fraction of the left hemisphere 1, 2 and 3 m after K18-PL aggregate injection in the frontal cortex. Both total and phosphorylated insoluble tau were detected for all 3 time points after K18-PL PFF injections, while very little to no insoluble tau was detected in the brain of buffer injected mice, thereby demonstrating unequivocal induction of tau pathology in the contralateral hemisphere as well (Fig. 4A). In the soluble brain fractions no significant differences were seen in total tau in buffer and

K18-PL injected mice (Fig. 4A). Western blotting and native gel electrophoresis from the left and right hemisphere of buffer and PFFs injected mice further confirm the ELISA results (Suppl Fig. 2–3).

Next, we investigated the spatial pattern of the developing tau pathology in the contralateral hemisphere. Sagittal brain slices were made at 3 different levels in the non-injected hemisphere (L −0.5 mm; −2.0 mm; −3.5 mm) of animals injected with PFF in the frontal cortex and used for AT8 IHC. AT8 positive tau pathology was detected in neurons of the non-injected hemisphere in a pattern that mirrored that of the injected hemisphere. At all 3 levels examined, we observed AT8 labeling of tangle-like aggregates in the frontal cortex and the hippocampus, which increased over time (Figs. 4B–C). Tau hyperphosphorylation is also clearly induced in the midbrain and brainstem (L −0.5 mm and −2.0 mm) 3 m after injection. Similarly tau pathology was observed in the contralateral hemisphere of mice injected with PFFs in the hippocampus in a pattern that mirrored that of the injected hemisphere (Suppl Fig. 4). Overall, these data indicate that the tau pathology spreads throughout the brain, with pathology spreading within a hemisphere to areas connected to the injected brain region and between hemispheres that are connected *via* commissural pathways such as the corpus callosum.

Onset of PFFs-induced tau pathology

Since maximal tau pathology is observed in the ipsilateral hemisphere of K18-PL PFF injected tauP301L mice from 1 m post-injection onwards, we next investigated tau hyperphosphorylation and aggregation at earlier time points after K18-PL PFF injection (2 days–1 m). In mice injected with K18-PL PFFs in the hippocampus (Fig. 5A) and cortex (Fig. 5B), very little to no phosphorylated tau (AT8) was detected in the sarkosyl-insoluble brain fractions of the injected and contralateral hemisphere 2 days after K18-PL PFF injection. The amount of insoluble phosphorylated tau gradually increased over longer post-injection survival intervals in both hemispheres; however, the injected hemisphere showed an earlier onset and a higher AT8 signal for all time points investigated. This indicates a clear time-dependent onset and spread of tau pathology in both hemispheres. AT8 IHC at the level of injection further confirms these findings (Figs. 5C and D).

To investigate the dynamics of the K18-PL PFF seeds, a myc antibody was used to detect the injected K18-PL aggregates. Myc IHC was performed on sagittal brain sections in both the injected and contralateral hemisphere and revealed a clear signal around the site of injection 2 days after K18-PL PFF injection in the hippocampus (Fig. 5E) or the frontal cortex (Fig. 5F). At later time points (1 week– 1 m), when clear induction of tau pathology was evident, the myc immunolabeling was undetectable at the hippocampal and cortical injection sites. Furthermore, no myc IHC was detected in the contra-lateral hemisphere after K18-PL injection in the hippocampus and the cortex during the 4 time points studied here (data not shown). Together, these data are suggestive of a limited diffusion of the seed and further corroborates the prion-like spreading mechanism of tau pathology.

Induction of tau pathology is dose- and time-dependent

To assess whether the amount of injected PFFs influenced the induction of tau pathology, we injected different doses of K18-PL PFFs (0.05– 25 μg) in the frontal cortex of tauP301L mice and dissected their brains at different time points after injection (1 week–2 m). Analysis of total and phosphorylated tau in sarkosyl-insoluble brain fractions of the injected and contralateral hemisphere revealed an increased tau signal with increasing amount of injected fibrils for the 4 time points (Fig. 6A). All investigated doses (0.5–25 μg) showed an increase in total and phosphorylated insoluble tau 1 and 2 weeks after injection, but the effect seems to level off from 1 m onwards. These data indicate that the induced tau pathology is influenced by both the injected dose of PFFs and the post-injection interval. However, the initial seeding at the site of injection seems to cause local aggregation that accounts for the majority of the signal.

To investigate whether it is necessary for the K18-PL to be fibrillar in order to induce tau pathology, *in vitro* fibrillized (PFFs) and non-fibrillized K18-PL were injected in tauP301L mice and total and phosphorylated tau was quantified in the sarkosyl-insoluble brain fractions 1 m after injection. Only PFFs-injected animals demonstrated an induction of insoluble total and phosphorylated tau, indicating the importance of aggregation status of the seed to induce tau pathology in the recipient mouse (Fig. 6B).

Next, we assessed the role of the P301L mutation in the human tau protein expressed in the recipient mouse. For this purpose, tau2N4R mice expressing the longest wild type human tau isoform without the P301L mutation and non-transgenic mice of the same genetic background as the transgenic mice (FvB/N) were injected with PFFs in the hippocampus. In contrast to the P301L mice, no significant increase in the amount of tau (total or phosphorylated) was present in the sarkosyl-insoluble brain fractions 3 m after injection (Fig. 6C). These results emphasize the importance of the P301L mutation for the rapid induction of tau pathology in the tau PFF injected mice. It remains to be investigated if over time the wild-type or tau4R mice will develop tau pathology as reported previously (Clavaguera et al., 2009).

Intracerebral injection of K18-PL PFFs induces inflammation

Since neuroinflammation is an important feature of pathology in Alzheimer's disease, we next investigated neuroinflammation in our seeding model. To investigate the presence of reactive astrocytes and activated microglia in K18-PL PFF injected mouse brain IHC for GFAP and Iba1 was performed on sagittal brain sections at the level of injection.

Two days after hippocampal injection, moderate astrogliosis was observed in both buffer and K18-PL injected mice (Figs. 7A; a, b). This is due to the surgical procedure itself, as the astrocyte response was also observed in buffer injected mice. In buffer injected animals, the inflammatory reaction decreased with time and only limited GFAP labeling was observed 1 m after injection (Figs. 7A; e). Animals injected with PFFs also displayed milder astrogliosis 2 weeks after injection when compared to earlier time points (Figs. 7A; b–d). However, at 1, 2 and 3 m after injection, the CA1 region of the hippocampus displayed strong astrogliosis (Figs. 7A; f–h, Fig. 7B). At these time points a major part of the CA1 neurons was also AT8

positive demonstrating that tau pathology is associated with strong and stable astrogliosis in the hippocampal neurons. Similarly, the tau pathology around the site of injection in K18-PL PFFs cortex-injected mice is associated with strong astrogliosis (Fig. 7C).

Mild microgliosis was observed in the hippocampus 2 days after hippocampal injection of buffer or K18-PL PFFs (Figs. 7D; a–b). While little or no microgliosis was observed in the hippocampus 1 week after injection of buffer, mild microgliosis was observed in the CA1 region of the hippocampus and a pronounced inflammatory reaction was observed in the corpus callosum 1 and 2 weeks after injection of K18-PL PFFs (Figs. 7D; c,d,e arrowhead). The most prominent proliferation and activation of microglia (based on the swollen morphology) was detectable in CA1 region 1 m after injection (Figs. 7D; f, Fig. 7E). Activated microglia infiltrated between the numerous AT8-positive neurons in the CA1 region (Figs. 7D, inset in f). Two and three months after injection, the number of reactive microglia decreased (Figs. 7D; g,h, Fig. 7E). In mice injected with K18-PL PFFs in frontal cortex, we also observed a higher amount of activated microglia around the injection site (Fig. 7F) compared to buffer injected animals. Interestingly, microglial activation was not restricted to the frontal cortex, but was also slightly increased in other regions affected by tau pathology (see Fig. 2D–E for AT8 IHC), such as the hippocampus, thalamus, amygdala and brainstem.

Overall, these data indicate that injections of K18 PFFs initiated neuroinflammation especially around the site of injection in both hippocampus and cortex of injected mice.

Intracerebral injection of K18-PL PFFs induced selective neuronal loss in the hippocampus

Prompted by the observation that AT8 and ThioS labeling was reduced over time in the hippocampus of PFF injected mice (Fig. 2C, Fig. 3B), we assessed whether there was neuronal loss in this area after injection of K18-PL PFFs. For this purpose, we performed Nissl staining on sagittal brain sections at the level of injection (L + 2,0 mm) and observed a decrease in Nissl stained neurons specifically in the hippocampal CA1 region (Fig. 8A). Quantification revealed that whereas CA1 neuron counts were unchanged 1 m after PFF injection, the number of neurons was clearly reduced 2 m after PFFs injection compared to buffer controls, and further decreased 3 m post-injection (Fig. 8B). Similarly, the length and volume of the CA1 region were measured in Nissl stained sections and a clear reduction was observed 2 and 3 m after injection (data not shown). The results were confirmed by NeuN labeling, which also showed decreased numbers of neurons with increasing post-injection survival intervals (Fig. 8C, Suppl Fig. 5). Interestingly, dual labeling with NeuN and AT8 revealed that while no neuronal cell loss was observed 1 m post-injection, there was unequivocal tau pathology as demonstrated by AT8 labeling, thereby indicating that tau pathology precedes the neuronal loss. Nissl staining of the contralateral hemisphere (L −2.0 mm) revealed no significant decrease in the number of CA1 neurons (data not shown). Since the amount of tau pathology in the hippocampus of the contralateral hemisphere was much lower than in the injected hemisphere, we surmise the neuron loss is driven by the burden of tau pathology and that it might take longer for hippocampal neurons to show evidence of degeneration until a threshold is reached that triggers this. Furthermore, injection of K18-PL

PFFs in the hippocampus of wild-type mice did not induce neuronal cell death, ruling out that the injected seed is causing neuronal loss independent of the occurrence of tau pathology (data not shown). NeuN and Nissl stainings were also performed in the frontal cortex of animals which received cortical infusion of PFFs, however, no cell loss was observed up to 3 m after seeding (data not shown). Together, these results suggest that tau aggregation induces neuronal death in our hippocampus injection model, albeit restricted to the CA1 region. This model thus provides the first described *in vivo* system of seeded tau pathology and transmission with at least in the hippocampus consequent neurodegeneration.

Discussion

Our data demonstrate that a single injection of tau PFFs in the hippo-campus or frontal cortex of young tauP301L mice acts as a seed to induce widespread tau pathology throughout the mouse brain, pointing to a tau prion-like spreading mechanism. This confirms previous *in vivo* data on the induction of tau fibrillization and spreading of pathology (Clavaguera et al., 2009; Lasagna-Reeves et al., 2012; Iba et al., 2013; Ahmed et al., 2014) and extends these findings through the utilization of a different tau Tg mouse model. Clear induction of tau pathology was observed around the site of injection, as well as in connected brain areas distant from these injection sites. This included the contralateral hemisphere, where clear tau pathology was observed in a pattern mirroring the injected hemisphere. Since tau pathology was detected in the contralateral hemisphere, this indicates that tau aggregates can spread between hemispheres through brain commissures such as the corpus callosum, and possibly also smaller anterior, posterior and hippocampal commissures. Furthermore, the increasing tau pathology in the more distant connected brain areas with increasing times after PFFs injection further points to prion-like spreading mechanisms in the formation of tau pathology. Our data also contribute to the increasing evidence that prion-like transmission of misfolded proteins represents a common process in the pathogenesis of several neurode-generative diseases, including α-synuclein in Parkinson's disease (Luk et al., 2012a, 2012b; Masuda-Suzukake et al., 2013), Aβ in AD (Walker et al., 2002; Meyer-Luehmann et al., 2006; Eisele et al., 2009) and SOD1 and TDP-43 in ALS (Polymenidou and Cleveland, 2011).

Previous *in vitro* data on tau spreading already showed that exogenously supplied synthetic tau preformed fibrils (PFFs) are taken up by cells, likely *via* endocytosis, and thereby act as “seeds” to induce aggregation of intracellular tau (Frost et al., 2009; Nonaka et al., 2010; Guo and Lee, 2011; Wu et al., 2013; Holmes et al., 2013). PFFs serve as a nucleus to which endogenous tau proteins are directly recruited, resulting in an amplified aggregation and propagation process (Friedhoff et al., 1998; Xu et al., 2010). Tau aggregates released from dying cells, *via* exosomal release or through some other undefined mechanism (Saman et al., 2012; Simón et al., 2012; Chai et al., 2012) may thus access surrounding healthy neurons and induce fibrillization of soluble tau. Furthermore, studies by Liu et al. (2012a), de Calignon et al. (2012) demonstrated that tau pathology can spread along anatomically connected networks, providing a likely explanation of the spread of tau pathology observed in our PFF injection model.

A key observation in this study is the induction of neuron loss in the hippocampal CA1 region of tauP301L mice injected with tau PFFs in the hippocampus. Until now, no neurodegeneration as a consequence of seeding-induced tau pathology has been described, although cell loss is an important characteristic in AD and related tauopathies. In this study, we were able to observe a significant loss of CA1 neurons 2 and 3 m after tau PFF injections in the hippocampus (a loss of 40% after 2 m and almost 60% after 3 m). No neuronal loss was observed after injection in the cortex, although more robust tau pathology was observed. In contrast,Clavaguera et al. (2009) andIba et al. (2013) found no significant neuron loss after hippocampal injections at post-injection intervals of up 6 m. Small differences in experimental design might account for the conflicting results, but the observed differences are hypothesized to be related to genetic background differences in the mouse strains employed in these different studies. For example, previous reports indicate that the excitotoxic effects of kainic acid (KA) in mouse hippocampus are strain dependent (Schauwecker and Steward, 1997; Mckhann et al., 2003; Liu et al., 2012b). Following KA administration, the extensive hippocampal cell loss is induced in the FvB/N mouse, while the pyramidal cells of other strains (for example C57BL/6 (B6)) are largely spared. Since the Tg tauP301L mice used in our study have an FvB/N background and the PS19 tau Tg mice used in the Iba et al. study are maintained on a B6C3 background, different susceptibility of the hippocampal neurons to tau toxicity might reflect an increased endogenous excitotoxic vulnerability in the FvB/N background. Such increased excitotoxic vulnerability could also explain the observed region specific neuronal vulnerability in our study, since hippocampal neurons are known to be most vulnerable to excitotoxic insults (Schauwecker and Steward, 1997; Mckhann et al., 2003; Liu et al., 2012b). In this regard, previous studies have indicated a role for synaptic dendritic tau in the regulation of neuronal excitability. Reduction of endogenous tau decreases susceptibility to excitotoxic seizures *in vivo* and reduces hyperexcitability in AD models overexpressing Aβ (Roberson et al., 2007, 2011; Holth et al., 2013). Tau is thought to mediate Aβ toxicity by interacting with the kinase Fyn. Fyn phosphorylates the NMDA receptor subunit NR2, facilitating the interaction with post-synaptic density protein 95 (PSD-95) that then leads to excitotoxic downstream signaling (Ittner et al., 2010; Roberson et al., 2011). The possibility that tau aggregation-induced cell loss observed in our PFF injection model is mediated by excitotoxic signaling merits further investigation.

Another important observation is the induction of inflammation in our tau PFF injection model. Numerous studies have documented the presence of inflammatory markers, such as pro-inflammatory cytokines and chemokines, as well as activated microglia, in damaged regions in the AD brain (reviewed by Akiyama et al., 2000; Lee et al., 2010), suggesting that there is a close correlation between neuroinflammation and AD pathogenesis. Furthermore, inflammation was shown to play a role in the events leading to neurodegeneration in tau Tg P301S mice (Bellucci et al., 2004; Yoshiyama et al., 2007). Despite the importance of inflammation in tau-induced neurodegeneration, the previously published tau injection models by Clavaguera et al.(2009),Iba et al.(2013) reported no increase in inflammatory mediators. In our study, however, abundant astrogliosis and microgliosis were observed after PFF injection, closely correlating with the induced tau pathology. The differences in glial response between these studies may be attributable to the different mouse strains that

were employed. Similar to our data, Ahmed et al. (2014) identified a subtle increase in microgliosis in tau tg mice 2.5 m after infusion with P301S brain extract. Despite no obvious nerve cell loss in this model, the increase in Iba1 staining might be indicative of an early inflammatory response to neurodegeneration. Since neuroin-flammation occurs before we see apparent cell loss in our model, we hypothesize that aggregated tau stresses the neurons triggering microglial and astroglial phagocytosis as an early inflammatory response in a pathogenic mechanism.

Overall, the tau seeding and aggregation model presented in this study confirms previous publications on the importance of prion-like spreading mechanisms in neurodegenerative diseases. Furthermore, the observed inflammation and neurodegeneration, two important characteristics of Alzheimer's disease, contribute to a more complete *in vivo* tau aggregation and spreading model. This mouse model can be used to further investigate the mechanisms involved in fibrillization and propagation of tau pathology, and can help in the search for disease modifying treatments for Alzheimer's disease and related tauopathies.

Supplementary Material

Refer to Web version on PubMed Central for supplementary material.

Acknowledgments

This work was supported by the Institute for the Promotion of Innovation by Science and Technology (IWT120492) in Flanders.

Abbreviations

AD	Alzheimer's disease
FTDP-17	frontotemporal dementia with Parkinsonism linked to chromosome 17
NFT	neurofibrillary tangle
PFFs	preformed fibrils
Tg	transgenic

References

Ahmed Z, Cooper J, Murray TK, Garn K, McNaughton E, Clarke H, et al. A novel in vivo model of tau propagation with rapid and progressive neurofibrillary tangle pathology: the pattern of spread is determined by connectivity, not proximity. Acta Neuropathol. 2014; 127:667–683. [PubMed: 24531916]

Akiyama H, Barger S, Barnum S, Bradt B, Bauer J, Cole GM, et al. Inflammation and Alzheimer's disease. Neurobiol. Aging. 2000; 21:383–421. [PubMed: 10858586]

Arriagada PV, Growdon JH, Hedley-Whyte ET, Hyman BT. Neurofibrillary tangles but not senile plaques parallel duration and severity of Alzheimer's disease. Neurology. 1992; 42:631–639. [PubMed: 1549228]

Ballatore C, Lee VM, Trojanowski JQ. Tau-mediated neurodegeneration in Alzheimer's disease and related disorders. Nat. Rev. Neurosci. 2007; 8:663–672. [PubMed: 17684513]

Bellucci A, Westwood AJ, Ingram E, Casamenti F, Goedert M, Spillantini MG. Induction of inflammatory mediators and microglial activation in mice transgenic for mutant human P301S tau protein. Am. J. Pathol. 2004; 165:1643–1652. [PubMed: 15509534]

Bottelbergs A, Verheijden S, Van Veldhoven PP, Just W, Devos R, Baes M. Peroxisome deficiency but not the defect in ether lipid synthesis causes activation of the innate immune system and axonal loss in the central nervous system. J. Neuroinflammation. 2012; 9:61. [PubMed: 22458306]

Braak H, Braak E. Neuropathological stageing of Alzheimer-related changes. Acta Neuropathol. 1991; 82:239–259. [PubMed: 1759558]

Braak H, Thal DR, Ghebremedhin E, Del Tredici K. Stages of the pathologic process in Alzheimer disease: age categories from 1 to 100 years. J. Neuropathol. Exp. Neurol. 2011; 70:960–969. [PubMed: 22002422]

Chai X, Dage JL, Citron M. Constitutive secretion of tau protein by an unconventional mechanism. Neurobiol. Dis. 2012; 48:356–366. [PubMed: 22668776]

Clavaguera R, Bolmont T, Crowther RA, Abramowski D, Frank S, Probst A, et al. Transmission and spreading of tauopathy in transgenic mouse brain. Nat. Cell Biol. 2009; 11:909–913. [PubMed: 19503072]

de Calignon A, Polydoro M, Suárez-Calvet M, William C, Adamowicz DH, Kopeikina KJ, et al. Propagation of tau pathology in a model of early Alzheimer's disease. Neuron. 2012; 73:685–697. [PubMed: 22365544]

Eisele YS, Bolmont T, Heikenwalder M, Langer F, Jacobson LH, Yan Z, et al. Induction of cerebral β-amyloidosis: intracerebral versus systemic Aβ inoculation. Proc. Natl. Acad. Sci. U. S. A. 2009; 106:12926–12931. [PubMed: 19622727]

Friedhoff P, Von Bergen M, Mandelkow EM, Davies P, Mandelkow E. A nucleated assembly mechanism of Alzheimer paired helical filaments. Proc. Natl. Acad. Sci. U. S. A. 1998; 95:15712–15717. [PubMed: 9861035]

Frost B, Jacks RL, Diamond MI. Propagation of tau misfolding from the outside to the inside of a cell. J. Biol. Chem. 2009; 284:12845–12852. [PubMed: 19282288]

Goedert M. Tau gene mutations and their effects. Mov. Disord. 2005; 20(Suppl. 12):S45–S52. [PubMed: 16092090]

Goedert M, Jakes R. Mutations causing neurodegenerative tauopathies. Biochim. Biophys. Acta. 2005; 3:240–250. [PubMed: 15615642]

Gómez-Isla T, Hollister R, West H, Mui S, Growdon JH, Petersen RC, et al. Neuronal loss correlates with but exceeds neurofibrillary tangles in Alzheimer's disease. Ann. Neurol. 1997; 41:17–24. [PubMed: 9005861]

Guo JL, Lee VM. Seeding of normal Tau by pathological Tau conformers drives pathogenesis of Alzheimer-like tangles. J. Biol. Chem. 2011; 286:15317–15331. [PubMed: 21372138]

Holmes BB, DeVos SL, Kfoury N, Li M, Jacks R, Yanamandra K, et al. Heparan sulfate proteoglycans mediate internalization and propagation of specific proteopathic seeds. Proc. Natl. Acad. Sci. U. S. A. 2013; 110:E3138–E3147. [PubMed: 23898162]

Holth JK, Bomben VC, Reed JG, Inoue T, Younkin L, Younkin SG, et al. Tau loss attenuates neuronal network hyperexcitability in mouse and Drosophila genetic models of epilepsy. J. Neurosci. 2013; 33:1651–1659. [PubMed: 23345237]

Huyghe S, Schmalbruch H, De Gendt K, Verhoeven G, Guillou F, Van Veldhoven PP, et al. Peroxisomal multifunctional protein 2 is essential for lipid homeostasis in Sertoli cells and male fertility in mice. Endocrinology. 2006; 147:2228–2236. [PubMed: 16484321]

Iba M, Guo JL, McBride JD, Zhang B, Trojanowski JQ, Lee VM. Synthetic tau fibrils mediate transmission of neurofibrillary tangles in a transgenic mouse model of Alzheimer's-like tauopathy. J. Neurosci. 2013; 33:1024–1037. [PubMed: 23325240]

Ittner LM, Ke YD, Delerue F, Bi M, Gladbach A, van Eersel J, et al. Dendritic function of tau mediates amyloid-beta toxicity in Alzheimer's disease models. Cell. 2010; 142:387–397. [PubMed: 20655099]

Lasagna-Reeves CA, Castillo-Carranza DL, Sengupta U, Guerrero-Munoz MJ, Kiritoshi T, Neugebauer V, et al. Alzheimer brain-derived tau oligomers propagate pathology from endogenous tau. Sci. Rep. 2012; 2:700. [PubMed: 23050084]

Lee YJ, Han SB, Nam SY, Oh KW, Hong JT. Inflammation and Alzheimer's disease. Arch. Pharm. Res. 2010; 33:1539–1556. [PubMed: 21052932]

Liu L, Drouet V, Wu JW, Witter MP, Small SA, Clelland C, et al. Trans-synaptic spread of tau pathology in vivo. PLoS ONE. 2012a; 7:e31302. [PubMed: 22312444]

Liu L, Hamre KM, Goldowitz D. Kainic acid-induces neuronal degeneration in hippocampal pyramidal neurons is driven by both intrinsic and extrinsic factors: analysis of FVB/N7C57BL/6 chimeras. J. Neurosci. 2012b; 32:12093–12101. [PubMed: 22933793]

Luk KC, Kehm VM, Zhang B, O'Brien P, Trojanowski JQ, Lee VM. Intracerebral inoculation of pathological α-synuclein initiates a rapidly progressive neurode-generative α-synucleinopathy in mice. JEM. 2012a; 209:975–986.

Luk KC, Kehm V, Carroll J, Zhang B, O'Brien P, Trojanowski JQ, et al. Pathological α-synuclein transmission initiates Parkinson-like neurodegeneration in nontransgenic mice. Science. 2012b; 338:949–953. [PubMed: 23161999]

Masuda-Suzukake M, Nonaka T, Hosokawa M, Oikawa T, Arai T, Akiyama H, et al. Prion-like spreading of pathological α-synuclein in brain. Brain. 2013; 136:1128–1138. [PubMed: 23466394]

McKhann GM, Wenzel HJ, Robbins CA, Sosunov AA, Schwartzkroin PA. Mouse strain differences in kainic acid sensitivity, seizure behavior, mortality, and hippocampal pathology. Neuroscience. 2003; 122:551–561. [PubMed: 14614919]

Meyer-Luehmann M, Coomaraswamy J, Bolmont T, Kaeser S, Schaefer C, Kilger E, et al. Exogenous induction of cerebral β-amyloidogenesis is governed by agent and host. Science. 2006; 313:1781–1784. [PubMed: 16990547]

Nonaka T, Watanabe ST, Iwatsubo T, Hasegawa M. Seeded aggregation and toxicity of α-synuclein and tau: cellular models of neurodegenerative diseases. J. Biol. Chem. 2010; 5:34885–34898. [PubMed: 20805224]

Polymenidou M, Cleveland DW. The seeds of neurodegeneration: prion-like spreading in ALS. Cell. 2011; 147:498–508. [PubMed: 22036560]

Roberson ED, Scearce-Levie K, Palop JJ, Yan F, Cheng IH, Wu T, et al. Reducing endogenous tau ameliorates amyloid beta-induced deficits in an Alzheimer's disease model. Science. 2007; 316:750–754. [PubMed: 17478722]

Roberson ED, Halabisky B, Yoo JW, Yao J, Chin J, Yan F, et al. Amyloid-β/Fyn-induced synaptic, network, and cognitive impairments depend on tau levels in multiple mouse models of Alzheimer's disease. J. Neurosci. 2011; 31:700–711. [PubMed: 21228179]

Saman S, Kim W, Raya M, Visnick Y, Miro S, Saman S, et al. Exosome-associated tau is secreted in tauopathy models and is selectively phosphorylated in cerebrospinal fluid in early Alzheimer's Disease. J. Biol. Chem. 2012; 287:3842–3849. [PubMed: 22057275]

Schauwecker PE, Steward O. Genetic determinants of susceptibility to excitotoxic cell death: implications for gene targeting approaches. Proc. Natl. Acad. Sci. U. S. A. 1997; 94:4103–4108. [PubMed: 9108112]

Simón D, Garcia-Garcia E, Royo F, Falcón-Pérez JM, Avila J. Proteostasis of tau. Tau overexpression results in its secretion via membrane vesicles. FEBS Lett. 2012; 586:47–54. [PubMed: 22138183]

Spittaels K, Van den Haute C, Van Dorpe J, Bruynseels K, Vandezande K, Laenen I, et al. Prominent axonopathy in the brain and spinal cord of transgenic mice over-expressing four-repeat human tau protein. Am. J. Pathol. 1999; 155:2153–2165. [PubMed: 10595944]

Terwel D, Lasrado R, Snauwaert J, Vandeweert E, Van Haesendock C, Borghgraef P, et al. Changed conformation of mutant Tau-P301L underlies the moribund tauopathy, absent in progressive, nonlethal axonopathy of Tau-4R/2 N transgenic mice. J. Biol. Chem. 2005; 280:3963–3973. [PubMed: 15509565]

Vandermeeren M, Mercken M, Vanmechelen E, Six J, Van de Voorde A, Martin J, et al. Detection of proteins in normal and Alzheimer's Disease cerebrospinal fluid with a sensitive sandwich enzyme-linked immunosorbent assay. J. Neurochem. 1993; 61:1828–1834. [PubMed: 8228996]

Walker LC, Callahan MJ, Bian F, Durham RA, Roher AE, Lipinski WJ. Exogenous induction of cerebral beta-amyloidosis in betaAPP-transgenic mice. Peptides. 2002; 23:1241–1247. [PubMed: 12128081]

Wu JW, Herman M, Liu L, Simoes S, Acker CM, Figueroa H, et al. Small misfolded Tau species are internalized via bulk endocytosis and anterogradely and retrogradely transported in neurons. J. Biol. Chem. 2013; 288:1856–1870. [PubMed: 23188818]

Xu S, Brunden KR, Trojanowski JQ, Lee VM. Characterization of tau fibrillization in vitro. Alzheimers Dement. 2010; 6:110–117. [PubMed: 20298971]

Yoshiyama Y, Higuchi M, Zhang B, Huang S, Iwata N, Saido TC, et al. Synapse loss and microglial activation precede tangles in a P301S tauopathy mouse model. Neuron. 2007; 53:337–351. [PubMed: 17270732]

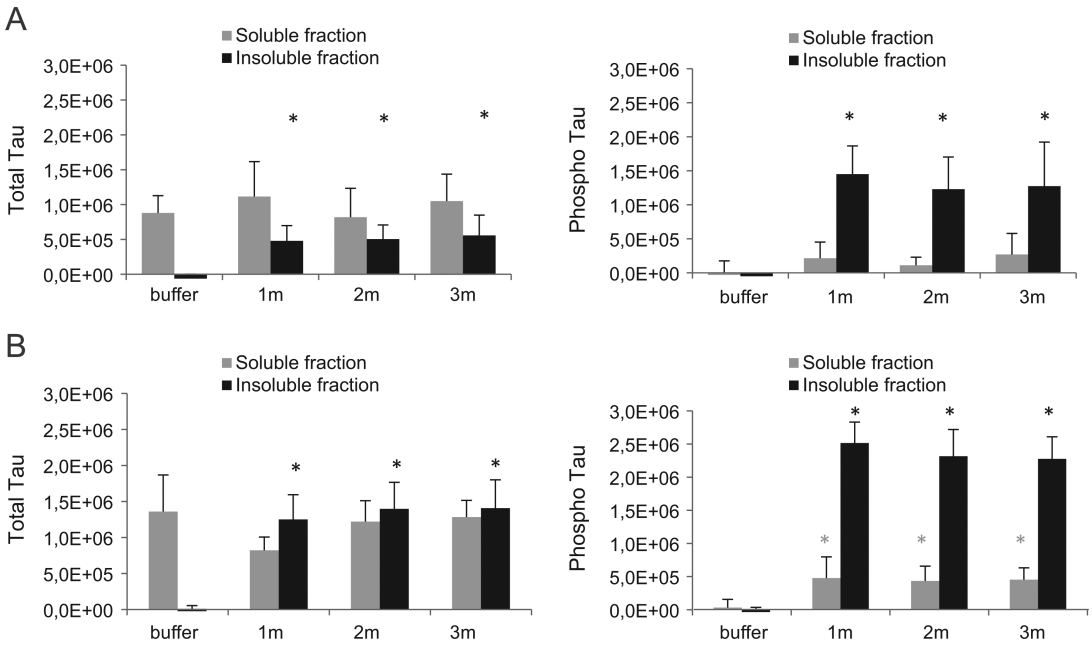

Fig. 1.

Total and phosphorylated tau in the ipsilateral hemisphere of mice injected with tau PFFs. Sarkosyl soluble and insoluble brain fractions of the whole injected (right) hemisphere were analyzed for total and phosphorylated tau by Elisa. Injection of K18-PL (25 μg) in the hippocampus (A) or frontal cortex (B) induces a clear increase in both total and phosphorylated insoluble tau compared to buffer injected mice. This increase is observed for all three time points (1 m–2 m–3 m after K18-PL injection). A small increase in phosphorylation is also observed in the soluble brain fraction of K18-PL injected mice. One-way Anova *$p < 0.05$ vs buffer ($n = 63$ m buffer, $n = 101$ m–2 m K18-PL, $n = 73$ m K18-PL).

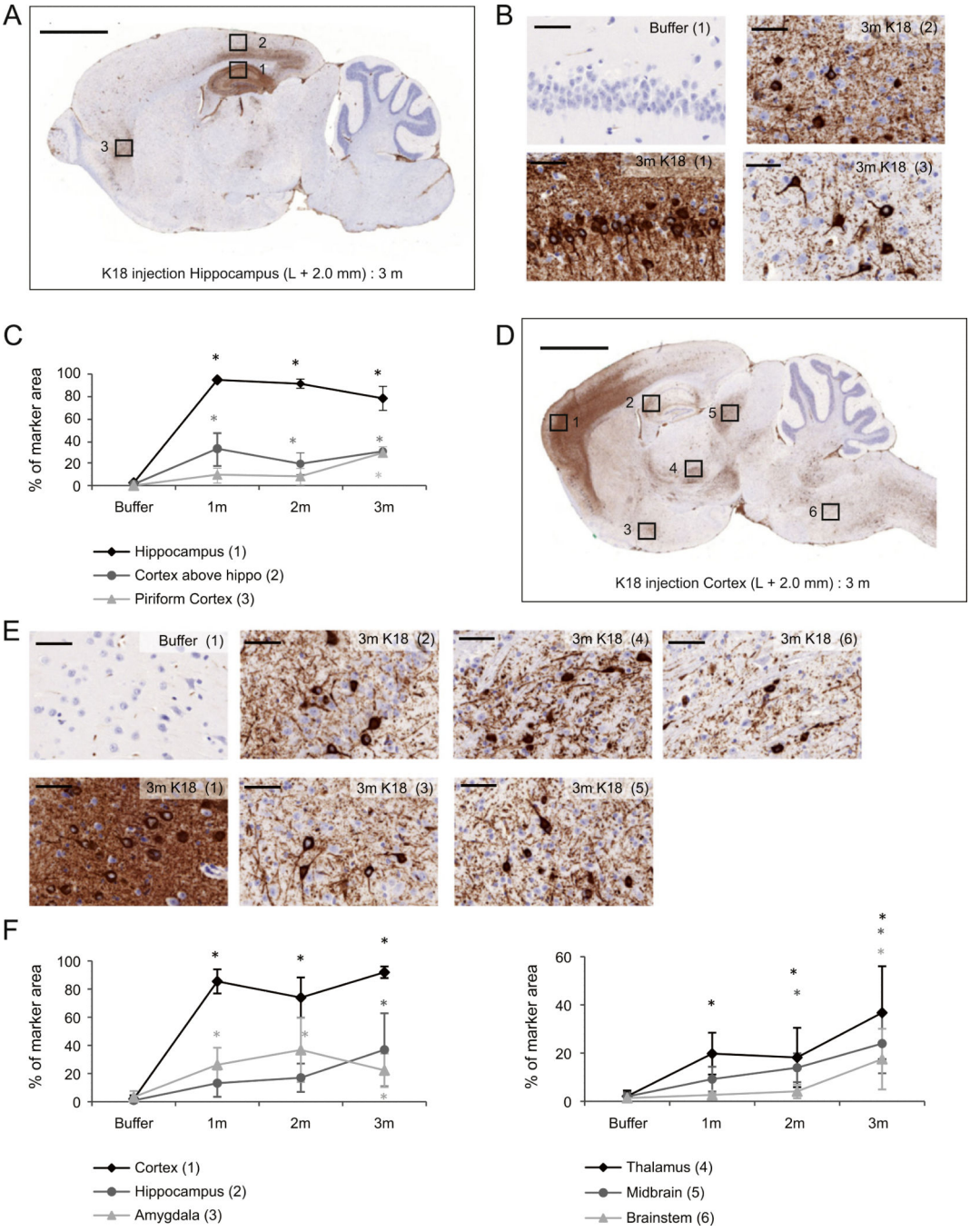

Fig. 2.

AT8 IHC in the ipsilateral hemisphere of mice injected with tau PFFs. (A) AT8 IHC on a sagittal brain section at the level of injection (L +2.0 mm) shows the distribution of tau pathology in the sagittal plane of an animal injected with K18-PL (25 μg) in the hippocampus. Scale bar: 2000 μm. (B) 40× magnification images of the indicated regions in A. Scale bars: 50 μm. (C) Quantification of the AT8 IHC reveals clear AT8 labeling in different regions of the K18-PL injected brains. One-way Anova *p < 0.05 *vs* buffer (n = 53 m buffer, n = 101 m–3 m K18-PL, n = 92 m K18-PL). (D) AT8 IHC on a sagittal brain

section at the level of injection (L +2.0 mm) of an animal injected with K18-PL (25 μg) in the frontal cortex. Scale bar: 2000 μm. (E) 40× magnification images of the indicated regions in D. Scale bars: 50 μm. (F) Quantification of the AT8 IHC reveals clear AT8 labeling in different regions of the K18-PL injected brains. One-way Anova *$p < 0.05$ *vs* buffer (n = 83 m buffer, n = 71 m K18-PL, n = 42 m K18-PL, n = 103 m K18-PL).

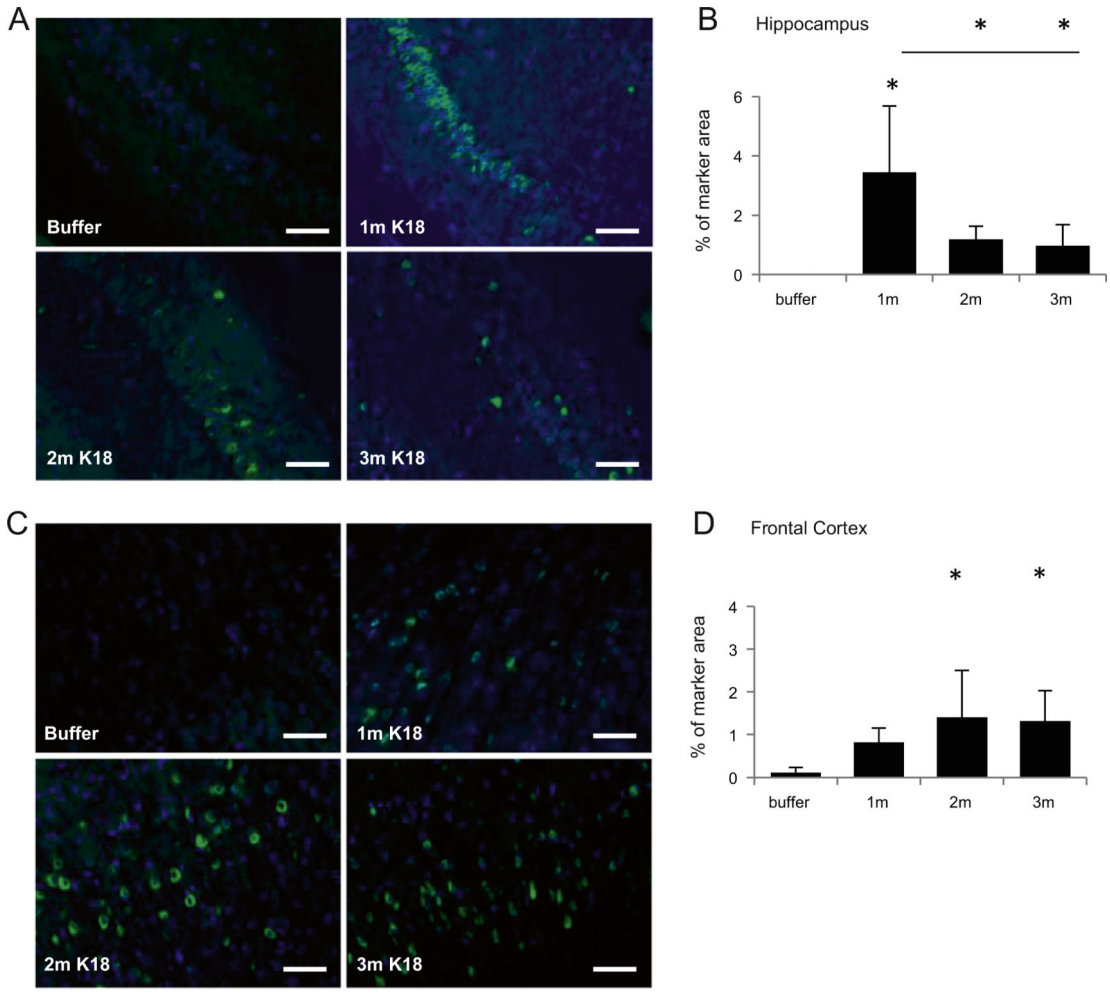

Fig. 3.

ThioS labeling in the ipsilateral hemisphere of mice injected with tau PFFs. (A) ThioS labeling in the hippocampus of animals injected with K18-PL (25 μg) in the hippo-campus. Scale bars: 100 μm. (B) Quantification of the ThioS labeling in the hippocampus reveals tau aggregates around the site of injection. One-way Anova *p < 0.05 *vs* buffer (n = 4 buffer, n = 101 m–2 m–3 m K18-PL). (C) ThioS labeling in the cortex of animals injected with K18-PL (25 μg) in the frontal cortex. Scale bars: 100 μm. (D) Quantification of the ThioS labeling in the frontal cortex reveals tau aggregates around the site of injection. One-way Anova *p < 0.05 *vs* buffer (n = 4 buffer, n = 61 m K18-PL, n = 42 m K18-PL, n = 93 m K18-PL).

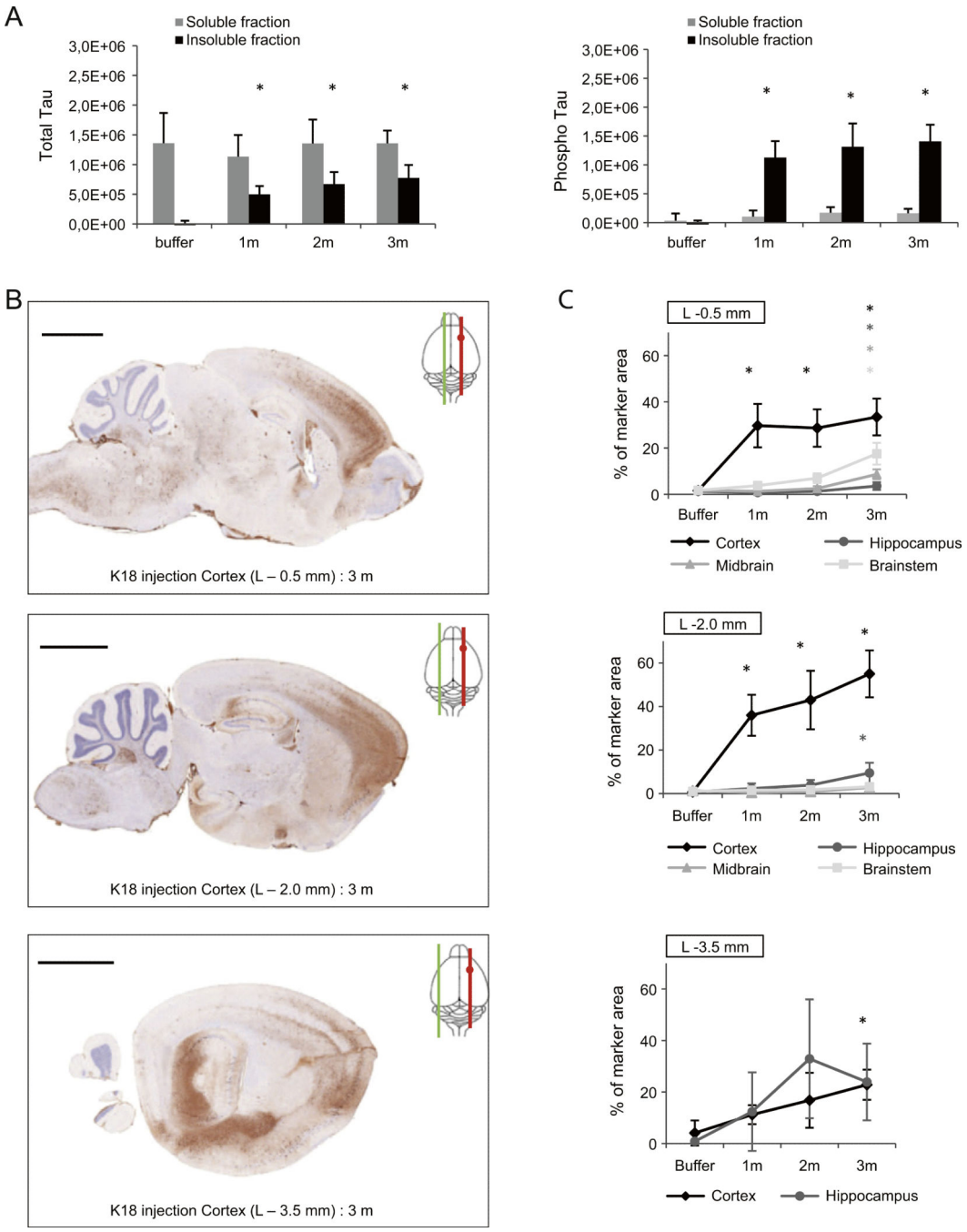

Fig. 4.

Tau pathology in the contralateral hemisphere of mice injected with tau PFFs. (A) Sarkosyl soluble and insoluble brain fractions of the non-injected (left) hemisphere of an animal injected with K18-PL (25 μg) in the frontal cortex were analyzed for total and phosphorylated tau by ELISA. K18-PL injected animals show a clear increase in both total and phosphorylated insoluble tau when compared to buffer injected mice. This increase is observed for all three time points (1 m–2 m–3 m after K18-PL injection). No significant differences were observed in total and phosphorylated soluble tau. One-way Anova *p <

0.05 *vs* buffer (n = 63 m buffer, n = 101 m–2 m K18-PL, n = 73 m K18-PL). (B) AT8 IHC on sagittal brain sections of the contralateral hemisphere at 3 different levels (L −0.5; −2.0; −3.5 mm) shows the distribution of the tau pathology in the coronal plane. Scale bars: 2000 μm. (C) Quantification of the AT8 IHC in multiple brain areas at the 3 different levels indicates clear tau pathology throughout the whole contralateral hemisphere. One-way Anova *p < 0.05 *vs* buffer (n = 33 m buffer, n = 71 m K18-PL, n = 42 m K18-PL, n = 93 m K18-PL).

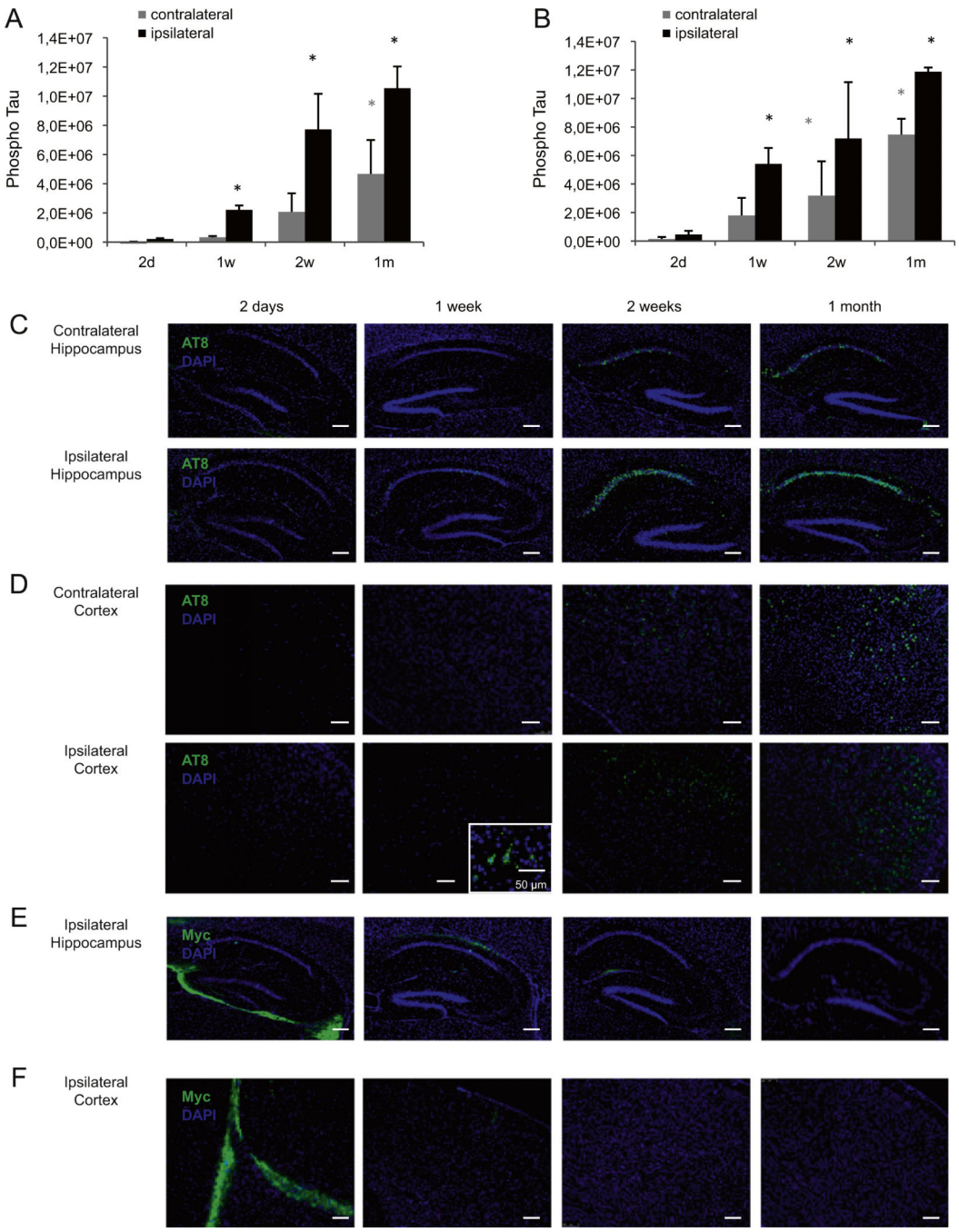

Fig. 5.

Early onset of tau pathology in mice injected with tau PFFs (A–B) Sarkosyl insoluble brain fractions of the injected and contralateral hemisphere were analyzed for phosphorylated tau at different time points (2 days–1 week) after injection of aggregated K18-PL (25 μg) in the hippocampus (A) or frontal cortex (B). Tau pathology is first observed in the injected hemisphere 1 week after injection and increases up to 1 m after injection in both hippocampus and cortex injected mice. The contralateral hemisphere shows a lower amount of tau phosphorylation and a later onset of pathology. One-way Anova *$p < 0.05$ *vs* 2 days

(n = 5/group). (C–D) AT8 immunohistochemisty in the hippocampus and frontal cortex of the injected (L +2 mm) and contralateral (L −2 mm) hemisphere confirms the biochemistry findings in animals injected with K18-PL in the hippocampus (C) and frontal cortex (D). (E–F) Myc labeling at the level of injection (L +2 mm) reveals a clear signal around the injection site 2 days after K18-PL injection in hippocampus (E) or frontal cortex (F). This signal decreases 1 and 2 weeks after injection and completely disappears 1 m post-injection. Scale bars: 250 μm.

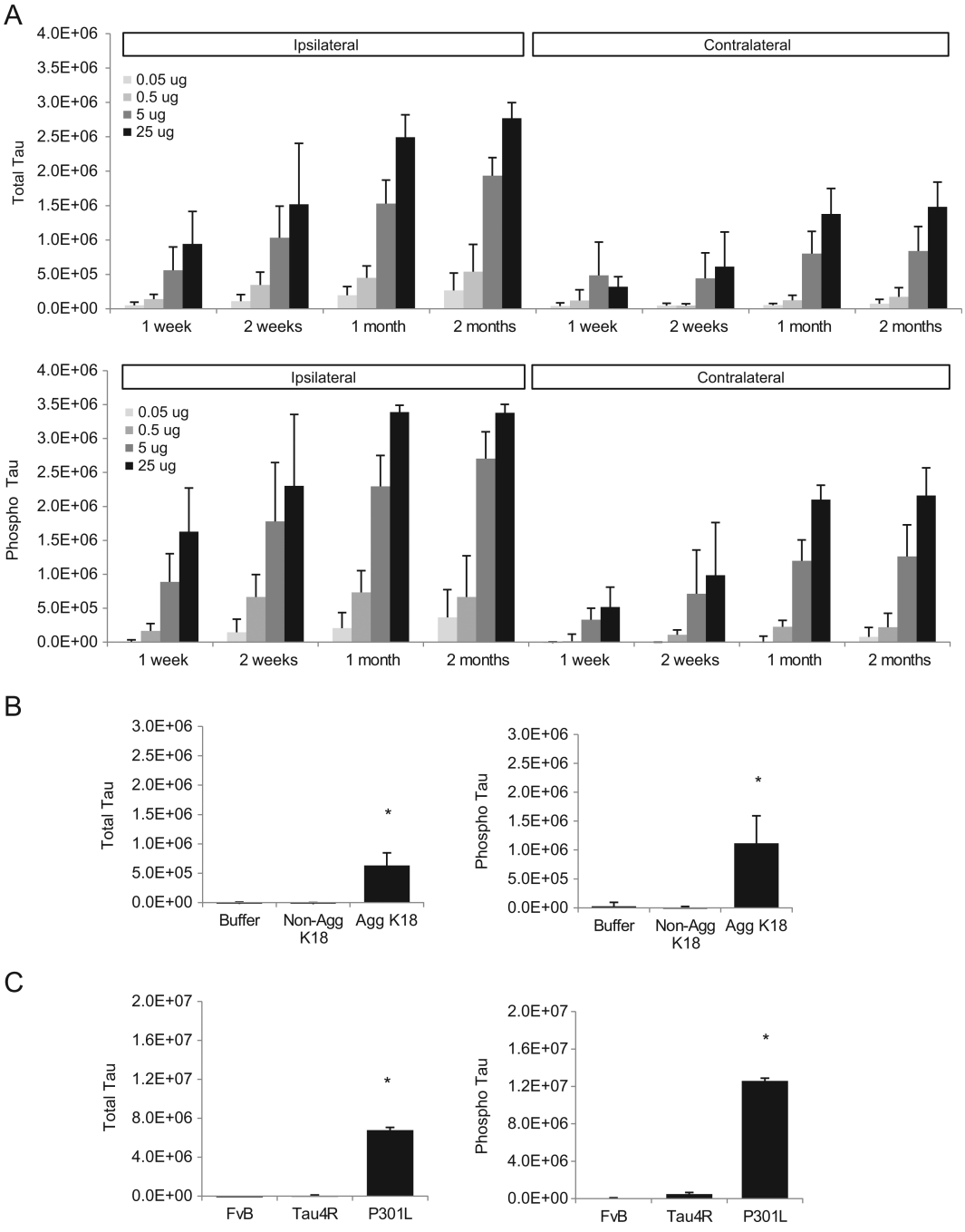

Fig. 6.

Induction of tau pathology is dose- and time-dependent. (A) Sarkosyl insoluble fractions of mouse brain injected with different amounts of aggregated K18-PL (0.05–25 μg) in the frontal cortex were analyzed for total and phosphorylated tau at different time points after K18-PL injection. In both the injected and contralateral hemisphere a dose-and time-dependent induction of tau pathology is observed (n = 5/group). (B) Mice injected with *in vitro* aggregated K18-PL (1 μg) in the cortex show a clear signal for total and phosphorylated Tau in their sarkosyl insoluble brain fractions one month after injection,

whereas no signal is observed in animals injected with buffer or non-aggregated K18-PL (1 μg). One-way Anova *p < 0.05 *vs* non-aggregated K18 (n = 9/group). (C) Injection of 25 μg aggregated K18-PL in the hippocampus of Tau4R or FvB mice does not cause a significant increase in the amount of total and phosphorylated tau in their sarkosyl insoluble brain samples one month after injection, whereas K18-PL injected P301L mice of a similar age clearly show induction of Tau pathology. One-way Anova *p < 0.05 *vs* Tau4R and *vs* FvB (n = 5 FvB; n = 6 Tau4R, n = 2 TauP301L).

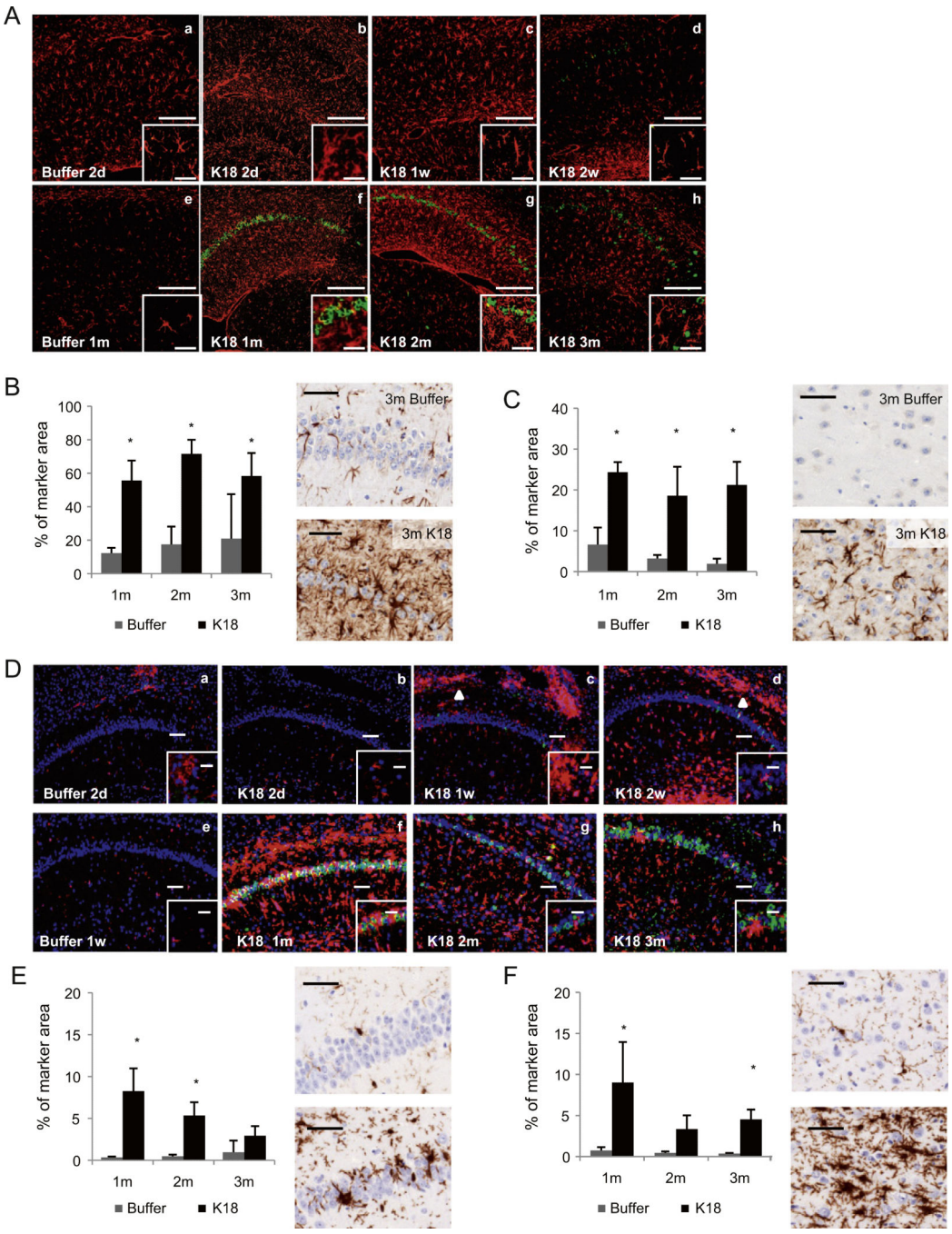

Fig. 7.

Intracerebral injection of tau PFFs induces astrogliosis and microgliosis. (A) GFAP (red) and AT8 (green) double IHC. Two days and 1 week after hippocampal injection, mild astrogliosis is observed in buffer (a) and K18-PL (b and c) injected animals. Two weeks after K18-PL injection, astrogliosis is milder (d), in comparison with earlier time points. One month after buffer injection, astrogliosis is virtually absent (e). At 1 m (f) 2 m (g) and 3 m (h) after K18-PL injection, massive proliferation and activation of astrocytes is observed, in combination with a strong increase in the amount of AT8 positive neurons. Scale bars: a–

h: 200 μm, inset: 50 μm. (B–C) GFAP labeling at the site of injection in animals injected with buffer or K18-PL (25 μg) in the hippocampus (B) or frontal cortex (C) reveals a clear increase in the number of astrocytes after K18-PL injection compared to buffer injection. Scale bars: 50 μm. One-way Anova * $p < 0.05$ *vs* buffer (B: n = 61 m–2 m buffer, n = 53 m buffer, n = 91 m K18-PL, n = 102 m and 3 m K18-PL; C: n = 61 m–2 m buffer, n = 83 m buffer, n = 71 m K18-PL, n = 42 m, n = 103 m K18-PL). (D) Iba1 (red) and AT8 (green) double IHC. Mild microgliosis is observed at the site of injection (a, b, c) and in the corpus callosum 1 week and 2 weeks after hippocampal K18-PL injection (c, d; arrowhead). Activated microglia are clearly detected 1 m after K18-PL injection (f), but decrease again 2 m (g) and 3 m (h) after K18-PL injection together with a decreasing number of AT8-positive neurons. Scale bars: a–h: 100 μm, inset: 50 μm. (E–F) Iba1 labeling at the site of injection in animals injected with buffer or K18-PL (25 μg) in the hippocampus (E) or frontal cortex (F) reveals a clear increase in the number of microglia after K18-PL injection compared to buffer injection. Scale bars: 50 μm. One-way Anova *$p < 0.05$ *vs* buffer (B: n = 61 m–2 m buffer, n = 53 m buffer, n = 101 m, 2 m and 3 m K18-PL; C: n = 61 m–2 m buffer, n = 83 m buffer, n = 71 m K18-PL, n = 42 m K18-PL, n = 103 m K18-PL).

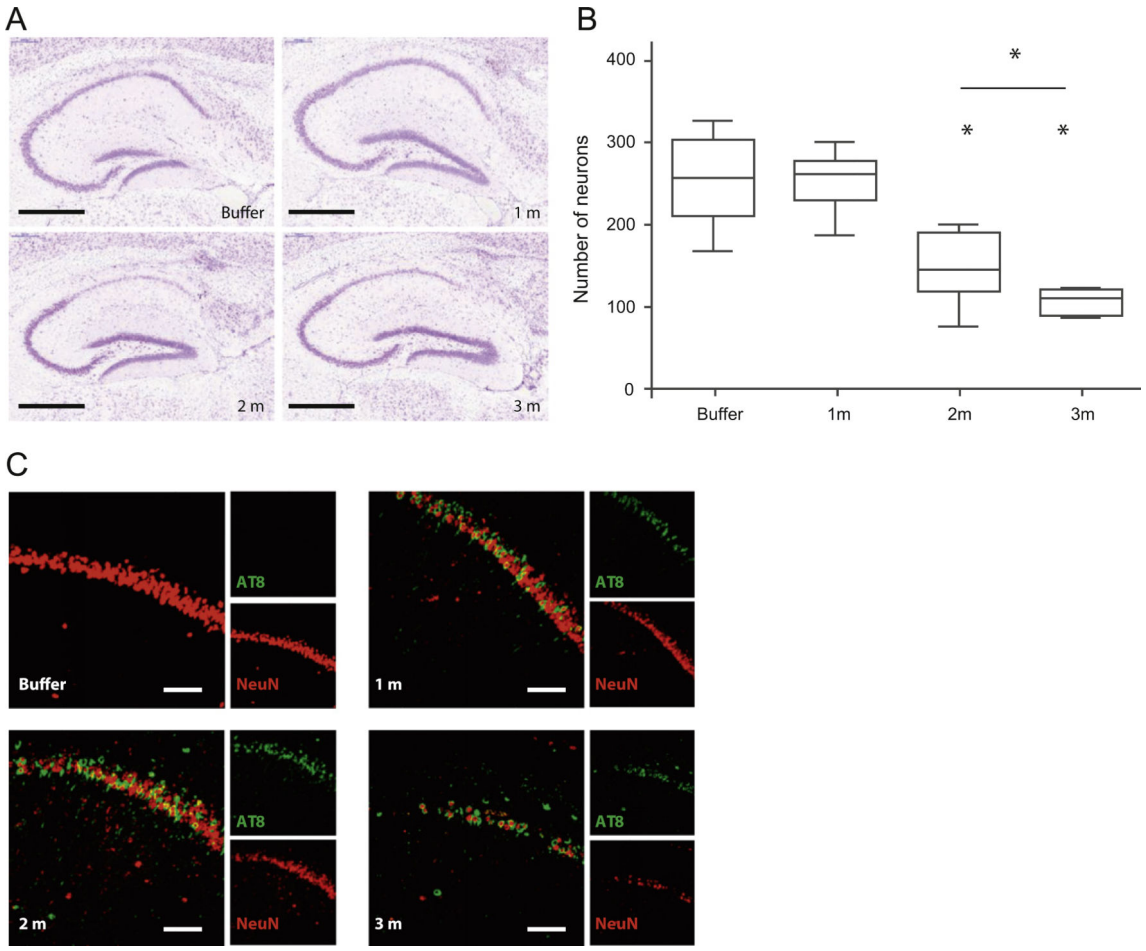

Fig. 8.

Injection of tau PFFs induces cell loss in the hippocampus. (A) Nissl staining in the hippocampus of P301L mice injected with buffer or aggregated K18-PL (25 μg) in the hippocampus. Scale bar: 500 μm. (B) Quantification of the number of Nissl-positive neurons in the CA1 region indicates a clear reduction in the number of neurons 2 and 3 m after K18-PL injection when compared to buffer injected mice. One-way Anova *$p < 0.05$ *vs* buffer, #$p < 0.05$ *vs* 2 m (n = 53 m buffer, n = 101 m en 3 m K18-PL, n = 82 m K18-PL). (C) AT8-NeuN double labeling in the hippocampus of K18-PL injected animals reveals a decrease in NeuN staining with increasing time after K18-PL injection. AT8-positive neurons are apparent 1 and 2 m after K18-PL injection, but this number is reduced 3 m after injection. Scale bars: 100 μm.